Lehrstuhl für
Technische Dynamik
Prof. Dr.-Ing. habil. Sigrid Leyendecker

Report
Chair of Applied Dynamics
2017

FRIEDRICH-ALEXANDER
UNIVERSITÄT
ERLANGEN-NÜRNBERG
TECHNISCHE FAKULTÄT

Prof. Dr.-Ing. habil. S. Leyendecker
Lehrstuhl für Technische Dynamik
Universität Erlangen-Nürnberg
Immerwahrstrasse 1
91058 Erlangen
Tel.: 09131 8561000
Fax.: 09131 8561011
www: http://www.ltd.tf.uni-erlangen.de

Editor: J. Rößler, D. Budday

Contents

1 Preface

This report summarises the activities in research and teaching of the Chair of Applied Dynamics at the University of Erlangen-Nürnberg between January and December 2017.

The main direction of research is computational dynamics and optimal control. Efficient technologies for dynamical and optimal control simulations are developed, facing contemporary life science and engineering problems. The problems under investigation come from biomechanics (natural or impaired human movements and athletic's high performance, human hand grasping, muscle wrapping) and robot dynamics (industrial, spatial and medical) as well as the optimisation and optimal control of their dynamics. Further topics are the modelling and simulation of biological and artificial muscles (as electromechanically coupled problems), multiscale and multirate systems with dynamics on various time scales (examples in astrodynamics as well as on the atomistic level), higher order variational integrators, Lie group methods and viscous beam formulations as well as research on structural rigidity and conformational analysis of macromolecules. The development of numerical methods is likewise important as the modelling of the nonlinear systems, whereby the formulation of variational principles plays an important role on the levels of dynamic modeling, optimal control as well as numerical approximation, yielding a holistic approach.

2 Team

chair holder
Prof. Dr.-Ing. habil. Sigrid Leyendecker

technical staff

Beate Hegen	
Dipl.-Ing. (FH) Natalia Kondratieva	until 31.07.2017
Sven Lässig	
Johannes Rößler	from 01.04.2017

academic scientist
Dr. rer. nat. Holger Lang

scientific staff

Dr. Toufik Bentaleb	from 15.08.2017
M.Sc. Dominik Budday	
Dr.-Ing Minh Tuan Duong	from 09.01.2017
M.Sc. Markus Eisentraudt	
M.Sc. Daniel Glaas	until 31.03.2017
Dipl.-Ing. Tobias Gail	until 31.12.2017
Dipl.-Ing. Thomas Leitz	
M.Sc. Johann Penner	
M.Sc. Uday Phutane	
Dipl.-Ing. Tristan Schlögl	
M.Sc. Theresa Wenger	

students

Dominik Bartels	Pascal Baysal
Felix Binder	Daniel Bretscher
Lewin Butazzo	Simon Dentler
Chaitanya Dev	Büsra Eris
David Fischer	Michèle Gleser
Alexander Greiner	Constantin Jehn
Simone Kellermann	Kilian Kleeberger
Björn König	Markus Lohmayer
Moritz Manert	Pirmin Molz
Nils Mößner	Arlette Ngnogue
Philip Nöh	Burak Ölcer
Mehdi Rezaiepour	Laura Ruhland
Sebastian Scheiterer	Karin Schol
Patrik Steck	Felix Töpfer
Minh Tam Truong	Prabhu Vijayan
Marcia Weigand	Thomas Will
Jinyu Zhang	Wuyang Zhao
Lukas Zikeli	

Student assistants are mainly active as tutors for young students in basic and advanced lectures at the Bachelor and Master level. Their contribution to high quality teaching is indispensable, thus financial support from various funding sources is gratefully acknowledged.


B. Hegen


N. Kondratieva


S. Lässig


J. Rößler


H. Lang


T. Bentaleb


D. Budday

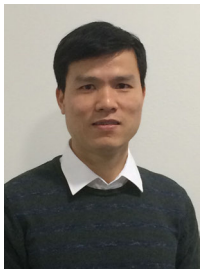
M. T. Duong

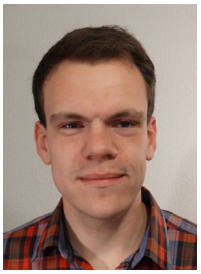
M. Eisentraudt


D. Glaas


T. Gail


T. Leitz

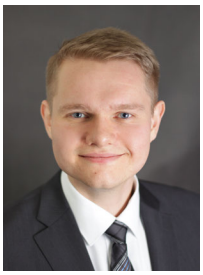
J. Penner

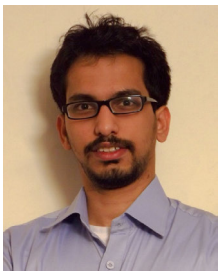
U. Phutane


T. Schlögl


T. Wenger


S. Leyendecker

3 Research

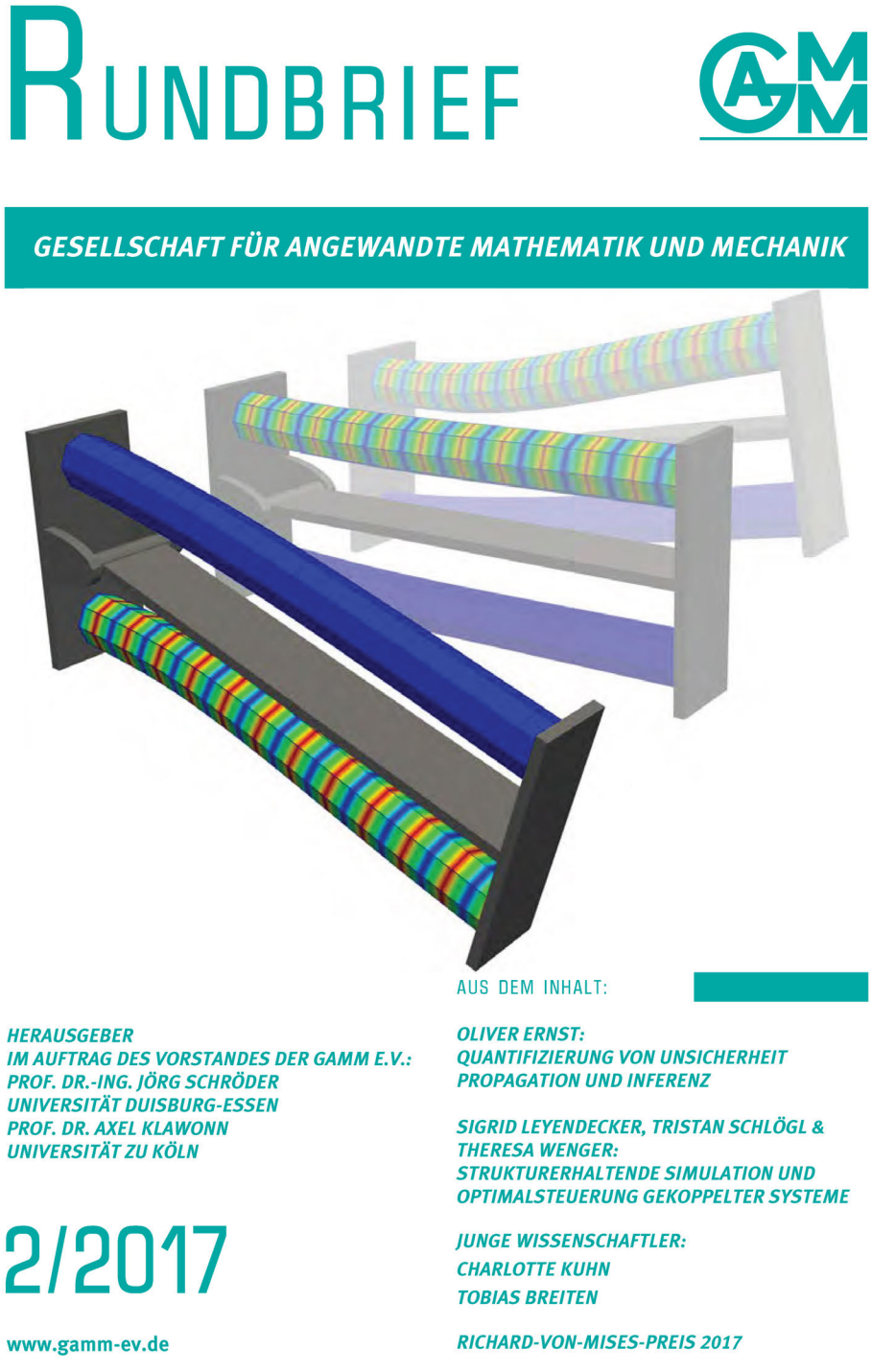
RUNDBRIEF
GAMM
GESELLSCHAFT FÜR ANGEWANDTE MATHEMATIK UND MECHANIK
AUS DEM INHALT:
HERAUSGEBER
IM AUFTRAG DES VORSTANDES DER GAMM E.V.:
PROF. DR.-ING. JÖRG SCHRÖDER
UNIVERSITÄT DUISBURG-ESSEN
PROF. DR. AXEL KLAWONN
UNIVERSITÄT ZU KÖLN
OLIVER ERNST:
QUANTIFIZIERUNG VON UNSICHERHEIT
PROPAGATION UND INFERENZ
SIGRID LEYENDECKER, TRISTAN SCHLÖGL &
THERESA WENGER:
STRUKTURERHALTENDE SIMULATION UND
OPTIMALSTEUERUNG GEKOPPELTER SYSTEME
JUNGE WISSENSCHAFTLER:
CHARLOTTE KUHN
TOBIAS BREITEN
RICHARD-VON-MISES-PREIS 2017
2/2017
www.gamm-ev.de

3.1 Biomechanics Workshop

On the 5. September, 2017, the Chair of Applied Dynamics (LTD) hosted a workshop on Biomechanics from participants affiliated to the LTD, lead by Prof. Sigrid Leyendecker and the Fraunhofer Institute for Industrial Mathematics (ITWM), headed by Dr. Joachim Linn. The workshop began with a talk from Dr. Michael Roller (ITWM) presenting his work on "Using optimal control to simulate the movement of assembly workers" and followed by a talk on behalf of his colleague, Mr. Marius Obentheuer (ITWM) on the topic "Application of muscle synergies in optimal control of a human arm model". The next talks were given on the topic of "Towards the optimal control of two finger grasping" by Mr. Uday Phutane (LTD), "Dynamic analysis with fuzzy uncertainty" by Mr. Markus Eisentraudt and "Control systems and robotics" by Dr. Toufik Bentaleb. The talks were followed by discussion on the theme 'Discrete Mechanics for Cosserat rods', followed by a nice dinner at ZEN Bar.

3.2 Rat heart project

The rat heart project is a research cooperation between the Chair of Applied Dynamics and the Pediatric Cardiology at University of Erlangen Nürnberg and is funded by the Klaus Tschira Stiftung. The goal of the project is to explore the heart function on pathological and normal conditions by developing a computational model of a rat heart which will be validated with realistic experiments at the Pediatric Cardiology. Consequently, a support heart system, for example, vascular assist system and/or artificial muscles can be properly designed and attached to and/or inserted into the rat heart for improving heart functioning, respectively. In the framework of the project, a research team is hence established to develop a computational heart model. Two master theses and one project thesis were completed with significant contributions. There are three ongoing master theses on the right tracks and the rat heart project still offers two more master topics concerning enhanced electrophysiological and excitation-contraction models for further investigations such as influence of the multiscale modelling (microscale such as cells and drugs to macroscale-tissue behaviour) on the heart function.

3.3 BMBF 05M2016 - DYMARA

The Federal Ministry of Education and Research (BMBF) promotes cooperation between universities and companies in the new funding priority 'Mathematics for Innovation'. 'Healthy Life' is the motto of the current promotional campaign. The joint project 05M2016 – DYMARA is coordinated by Professor Dr. Bernd Simeon from Technische Universität Kaiserslautern (UNIKL) and has a thematic relation to ergonomics and health promotion at work. The aim of the project is to develop an innovative digital human model with detailed skeletal muscle modelling and fast numerical algorithms for fundamental research. As part of the collaborative project, the LTD investigates muscle paths in the biomechanical simulation of human motion and the integration of new fiber-based muscle models to multi-body dynamics while the UNIKL is developing a continuum mechanical muscle model. The project partner Dr. Michael Burger from the Fraunhofer-Institut für Techno- und Wirtschaftsmathematik (ITWM) is focusing on the optimal control of the complete digital human model. Industrial partners are MaRhyThe-Systems GmbH & Co. KG. and flexstructures GmbH.

3.4 Scientific and academic honors

Holger Lang took the second place for his lecture 'Theoretische Dynamik' in the category VP5 as part of the Teaching Evaluation of the Sommersemester 2017.

3.5 Scientific reports

The following pages present a short overview on ongoing research projects pursued at the Chair of Applied Dynamics. These are partly financed by third-party funding (German Research Foundation (DFG), The Federal Ministry of Education and Research (BMBF), Bavarian Environment Agency (LfU), Deutsche Telekom Stiftung) and in addition by the core support of the university.

Research topics

Hierarchical, hydrogen bond encoded protein motions
Dominik Budday, Sigrid Leyendecker, Henry van den Bedem

Computational modelling of cardiac muscles of a rat heart
Minh Tuan Duong, Sigrid Leyendecker

A variational integrator for constrained mechanical systems with pulsed disturbances and optimal feedback control
Daniel Glaas, Sigrid Leyendecker

Numerical convergence analysis of higher order multi-symplectic Lie-group variational integrators for geometrically exact beam dynamics
Thomas Leitz, Sigrid Leyendecker

Optimal control of a slot car racer using a discrete variational principle
Johann Penner, Tristan Schlögl, Sigrid Leyendecker

Optimal control simulations of two finger grasping
Uday D. Phutane, Michael Roller, Sigrid Leyendecker

A polarisation based approach to model strain dependent electrostatic pressure of dielectric elastomer actuators
Tristan Schlögl, Sigrid Leyendecker

Variational integrators of mixed order for constrained multirate systems
Theresa Wenger, Sina Ober-Blöbaum, Sigrid Leyendecker

Hierarchical, hydrogen bond encoded protein motions

Dominik Budday, Sigrid Leyendecker, Henry van den Bedem[1]

Protein rigidity analysis can provide fast insights into conformationally coupled regions and flexibility in the molecule. However, common constraint-counting approaches to rigidity are based on the topological pebble game algorithm [1] and have two significant limitations. First, missing geometric information hides the kinematics of internal motions, restricting results to a number of degrees of freedom and flexibility indices. Second, the analysis is highly dependent on a set of non-covalent interactions used as input to rigidity analysis. Overall, this limits applicability and comparability to dynamic, normal mode analysis (NMA) or their simplified elastic network model (ENM) variants.
Here, we detail that the hydrogen bonding pattern, a common input to rigidity analysis, encodes a hierarchy of motions beyond the rigid cluster decomposition. Given the constraint Jacobian $\mathbf{J}$ with $5m$ hydrogen bond constraints and d dihedral angles, we identify two disjoint subspaces for joint velocities from the singular value decomposition (SVD) $\mathbf{JV} = \mathbf{U\Sigma}$, where $\mathbf{U} = [\mathbf{u}_1, \dots, \mathbf{u}_{5m}] =\in \mathbb{R}^{5m\times 5m}$ and $\mathbf{V} = [\mathbf{v}_1, \dots, \mathbf{v}_d] =\in \mathbb{R}^{d\times d}$. The rectangular matrix $\mathbf{\Sigma} = \text{diag}(\sigma_1, \dots, \sigma_p) \in \mathbb{R}^{5m\times d}, p = \min(5m, d)$ contains the singular values σ_i on the diagonal axis, where $\sigma_1 \geq \dots \geq \sigma_r > \sigma_{r+1} = \dots = \sigma_p = 0$ and r the rank of $\mathbf{J}$. The corresponding $\mathbf{u}_i$ and $\mathbf{v}_i$ are termed the ith left and right singular vector, respectively. Then, we term

$$\begin{aligned} \text{range}(\mathbf{J}^T) &= \text{span}\{\mathbf{v}_1, \dots, \mathbf{v}_r\} =: \mathbf{R}, \\ \text{null}(\mathbf{J}) &= \text{span}\{\mathbf{v}_{r+1}, \dots, \mathbf{v}_d\} =: \mathbf{N}, \end{aligned} \tag{1}$$

denoting the range $\mathbf{R}$ and nullspace $\mathbf{N}$, respectively. These two subspaces provide physically distinct insights. Since $\mathbf{u}_i$ and $\mathbf{v}_i$ are orthonormal vectors, σ_i represent non-orthogonality between $\mathbf{J}$ and $\mathbf{v}_i$. In other words, they encode the norm of constraint perturbation when moving along $\mathbf{v}_i$. For motions in $\mathbf{N}$, this perturbation is zero, encoded by the vanishing singular value. We have previously shown that the nullspace yields an identical, yet more informative rigid cluster decomposition [2] than traditional topological approaches, with the nullspace dimension representing the number of internal degrees of freedom, often termed floppy modes. The kinematics of these floppy modes, coupled to sophisticated motion planners with dynamic, Clash-avoiding Constraints (dCC) revealed conformational transitions in proteins [3], the role of secondary structure in RNA conformational changes [4], and coupled loop motions important for biological function in dehydrofolate reductase (DHFR) [5].

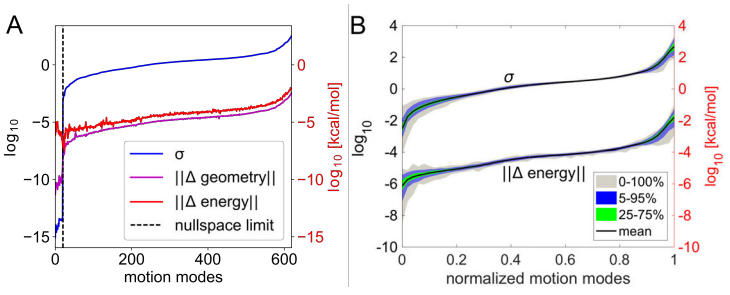

Figure 1: Singular values track geometric and energetic hydrogen bond perturbation, shown for one example (A, PDB ID 1p5f) and a large, diverse dataset with 183 proteins (B). Perturbations are computed from stepping along individual motion modes $\mathbf{v}_i$ (step size $1e-5$) and show a conserved distribution, displaying the predictive power of σ.

The range $\mathbf{R}$ of $\mathbf{J}^T$ provides a spectrum of motions ranked by increasing constraint perturbation. Consistent with the notion in penalty methods, the singular value $\sigma_i \geq 0$ denotes a penalty associated with collectively perturbing constraints when moving along singular vector $\mathbf{v}_i$. Interestingly, this

[1]Division of Biosciences, SLAC National Accelerator Laboratory, Stanford University, California, Menlo Park, USA

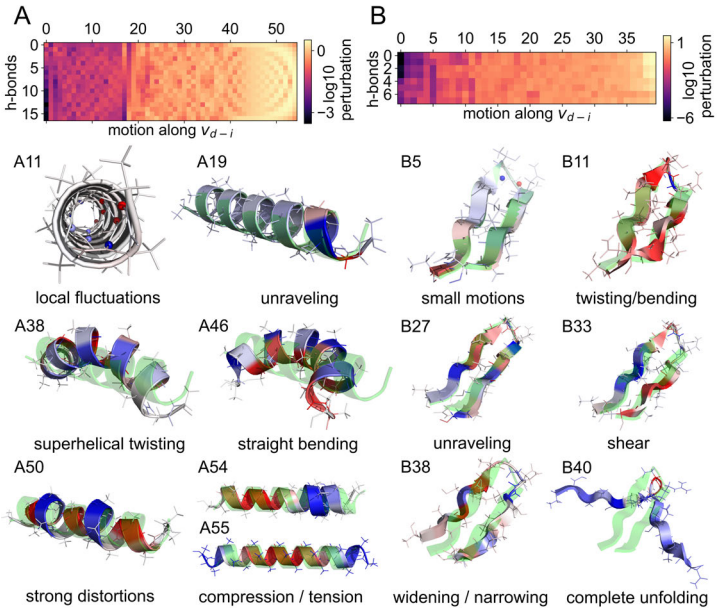

Figure 2: Hierarchical constraint perturbation in α-helices (A panels) and antiparallel β-sheets (B panels). The two top panels plot the matrix $\mathbf{JV}$, ranking singular vectors (columns) across individual hydrogen bonds (rows) and associated constraint perturbation in color increasing from purple to yellow. Bottom panels depict example motion modes from indicated columns, with increasing overall constraint perturbation. The color pattern follows associated entries in $\mathbf{v}_i$, showing increasing changes of degrees of freedom from blue to red.

penalty tracks collective hydrogen bond geometry and energy perturbations across a large set of proteins from the Protein Data Bank (PDB) (Fig. 1), computed from the geometric constraints and the Mayo potential [6], respectively. We physically demonstrate this hierarchy for an α-helix and a β-sheet (Fig. 2), ranging from local fluctuations to more collective motions such as superhelical twisting of the helix, or sheet shearing. Compression and tension in the α-helix perturb the hydrogen bonds significantly, suggesting unraveling as the more favorable mode of unfolding, which agrees with more detailed molecular dynamics simulations [7]. Overall, we expect this hierarchy to correlate with experimentally determined hydrogen-deuterium exchange and be related to temperature-based fluctuations in the molecular free-energy landscape.

References

[1] D. J. Jacobs and M. F. Thorpe, *Generic rigidity percolation: the pebble game.* Phys Rev Lett **75**, 4051 (1995).

[2] D. Budday, S. Leyendecker and H. van den Bedem, *Geometric analysis characterizes molecular rigidity in generic and non-generic protein configurations.* J Mech Phys Solids **83**, 36–47 (2015).

[3] D. Budday, R. Fonseca, S. Leyendecker and H. van den Bedem, *Frustration-guided motion planning reveals conformational transitions in proteins.* Proteins: Struct, Funct, Bioinf **85**, 1795–1807 (2017).

[4] A. Héliou, D. Budday, R. Fonseca and H. van den Bedem, *Fast, clash-free rna conformational morphing using molecular junctions.* Bioinformatics, btx127 (2017).

[5] R. Fonseca, D. Budday and H. van den Bedem, *Collision-free poisson motion planning in ultra high-dimensional molecular conformation spaces.* J Comput Chem, JCC25138 (2018).

[6] B. I. Dahiyat, D. B. Gordon and S. L. Mayo, *Automated design of the surface positions of protein helices.* Protein Sci **6**, 1333–1337 (1997).

[7] M. J. Buehler and S. Keten, *Elasticity, strength and resilience: A comparative study on mechanical signatures of α-helix, β-sheet and tropocollagen domains. Nano Res.*, 1(1):63–71, (2008).

Computational modelling of cardiac muscles of a rat heart

Minh Tuan Duong, Sigrid Leyendecker

Computational modelling is essential to better understand the function of rat hearts under pathological and normal conditions. In this work, the electromechanics of cardiac muscles, which is the basis for the contraction of the heart, is addressed for a rat left ventricle (LV) and biventricular model (BV). A 3D geometry of a rat LV and a BV are first constructed from MRI images provided by the Pediatric Cardiology in Erlangen. Fibre orientation maps are then computed approximately for the LV and BV to account for cadiac muscle directions which are important for their orthotropic mechanical and electrical properties. Specifically, we use FitzHugh-Nagumo and Aliev-Panfilov models for the oscillatory pacemaker and non-oscillatory cardiac muscle cells to model electric potential based on the monodomain formulation [1]. Finally, the fully coupled model for the electromechanics of the LV and BV are developed by employing the active stress approach. Cardiac muscles are commonly aligned on sheet planes distributed in the ventricular wall hellically with respect to the longitudinal axis of the heart. Furthermore, the fibre angle with respect to the local circumferential direction varies from the endocardium to the epicardium, so-called boundary surfaces $\partial\mathfrak{B}_\theta$ (60° to -60° for rat). Consequently, the components of the fibre vector $\boldsymbol{f}_0$ and the sheet vector $\boldsymbol{s}_0$ can be interplolated through the ventricular wall-thickness by solving the Laplace equation for each scalar-component value θ of these vectors; $\Delta\theta = 0$ in $\mathfrak{B}$ with the Dirichlet boundary conditions $\theta = \bar{\theta}$ on $\partial\mathfrak{B}_\theta$ [2], see Figure 1. A structurally based passive material law (Holzapfel-Ogden) for the LV and BV is described as

$$W = \frac{a}{2b} e^{b(I_3-3)} + \sum_{i=f,s} \frac{a_i}{2b_i} \left[e^{b_i (I_{4i}-1)^2} - 1 \right] + \frac{a_{fs}}{2b_{fs}} \left[e^{b_{fs} \left(I_{8fs}\right)^2} - 1 \right], \tag{1}$$

where a, b, a_i, b_i, for $i = s, f$ and a_{fs}, b_{fs} are material constants; I_3, I_{4i}, and I_{8fs} are the invariants of the right Cauchy-Green tensor, see [3] .

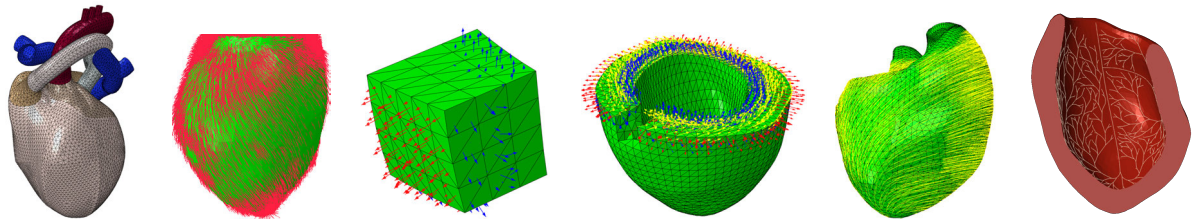

Figure 1: Whole heart mesh model, fibre orientations (LV and BV) and Purkinje network (LV).

The material parameters can be obtained by fitting the model to experimental data from mechanical testing, such as biaxial tests and shear tests. If the experiments provide sufficient information, the material constants are more accurate and the predictions of LV and BV behaviour are closer to reality. Furthermore, the fast conducting Purkinje fibre network is reconstructed for the LV and BV (Figure 1). This accounts for the synchronous activation of all muscle cells during a heartbeat. In addition, the electrical potential of the LV can be represented in a form of the reaction-diffusion equation (a parabolic problem) with oscillatory pacemaker (p) cells modelled by the FitzHugh-Nagumo and non-pacemaker (np) cells by the Aliev-Panfilov model

$$\dot{\phi} = \mathrm{Div}(\boldsymbol{q}) + f^{\phi}(\phi, r), \quad f_p^{\phi} = c[\phi[\phi - \alpha][\phi - 1] - r], \quad f_{np}^{\phi} = c\phi[\phi - \alpha][\phi - 1] - r\phi \tag{2}$$

$$\dot{r} = f^{r}(\phi, r), \quad f_p^{r} = \phi - br - a, \quad f_{np}^{r} = [\gamma + \frac{\mu_1 r}{\mu_2 + \phi}][-r - c\phi[\phi - b - 1]], \tag{3}$$

with action potential ϕ, recovery variable r, electric flux $\boldsymbol{q} = \mathbf{D} \cdot \nabla(\phi)$, conductivity tensor $\mathbf{D} = d_{iso}\mathbf{I} + d_{ani}\boldsymbol{f}_0 \otimes \boldsymbol{f}_0$, fibre unit vector $\boldsymbol{f}_0$, identity tensor $\mathbf{I}$, isotropic and anisotropic (along fibres) conduction d_{iso}, d_{ani} and model constants a, b, c, α, μ_1, and μ_2, see [1].

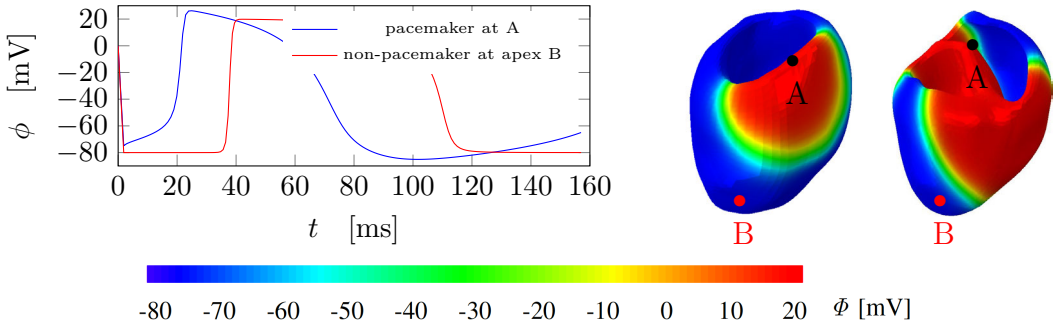

Figure 2: Potential of pacemaker cell at A, non-pacemaker cell at B (left), and the LV, BV (right).

The FitzHugh-Nagumo model is derived based on a phenomenological approach since it captures the potential evolution using only two variables describing the fast stroke and the relaxation phase. It is unable to investigate influences from the micro level (cells, drugs) on the macro level (muscle tissues).

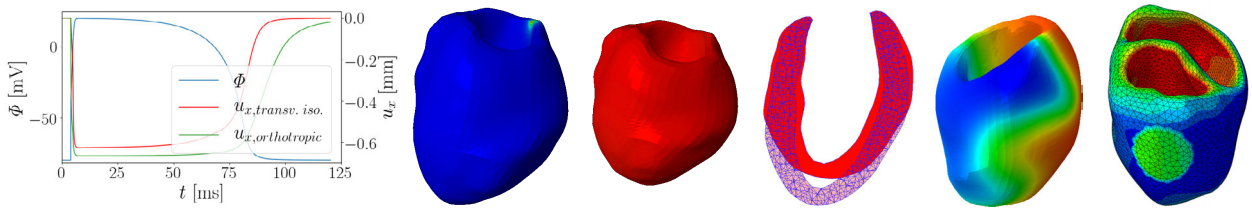

Figure 3: Displacement-potential curve (left), resting and contraction of the LV, section view, fibrillation and infarcted region (right).

A fully coupled model is obtained by coupling the equations (2) and (3) with the mechanical quasi-static form of the first Piola-Kirchhoff stress $\mathrm{Div}(\mathbf{P}) = \mathbf{0}$ in $\mathfrak{B}$. The excitation-contraction model is based on the active stress approach as $\mathbf{P} = \mathbf{P}_{pas} + \mathbf{P}_{act}(\boldsymbol{u}, T^{act})$ where the passive stress is $\mathbf{P}_{pas}$ and its active counterpart is $\mathbf{P}_{act}$ as a function of the displacement $\boldsymbol{u}$ and the active muscle traction T^{act} defined by $\dot{T}^{act} = \epsilon(\phi)[k_\sigma(\phi - \phi_r) - T^{act}]$, in which $\epsilon(\phi)$ determines a smooth activation, k_σ and ϕ_r control the maximum active force and resting potential, respectively. The active stress is introduced as a result of electrical stimulation $\mathbf{P}_{act} = T^{act}[\nu_{ff}\boldsymbol{f_0} \otimes \boldsymbol{f_0} + \nu_{ss}\boldsymbol{s_0} \otimes \boldsymbol{s_0}]$ where ν_{ff} and ν_{ss} are the weighting factors for active stress generation. In Figure 3, the results shows the interaction of excitation and contraction in the LV using the above electromechanical model. The fibrillation of the LV and an infarcted BV, which often occur in pathological conditions, is depicted in Figure 3 (right). To cure the disfunctions, the electrical wave needs to be stabilized by an artifical pacemaker. To improve the heart pumping ability the improvement and development of certain vascular assistant systems are necessary. Generally, in the next steps the numerical simulation results such as pressure-volume curves, displacements or potential can be compared with experimental data provided by the Pediatric Cardiology in Erlangen.

References

[1] S. Göktepe, and E. Kuhl. *Electromechanics of the heart: a unified approach to the strongly coupled excitation-contraction problem.* Comput Mech **27**, 227–243 (2010).

[2] J. Wong, and E. Kuhl. *Generating fibre orientation maps in human heart models using Poisson interpolation.* Computer Methods in Biomechanics and Biomedical Engineering, 1–10 (2012).

[3] G.A. Holzapfel, and R.W. Ogden. *Constitutive modelling of passive myocardium: a structurally based framework for material characterization.* Phil. Trans. R. Soc. A. **367**, 3445–3475 (2009).

A variational integrator for constrained mechanical systems with pulsed disturbances and optimal feedback control

Daniel Glaas, Sigrid Leyendecker

The following article provides a summary of [4], including literal excerpts.

Variational integrators and DMOC Today, a lot of mechanical systems have to operate with an improved performance compared to equal constructions decades ago. To stay competitive, engineers of a mechanical system need to guarantee its optimal operation. This includes both offline optimisation of a desired trajectory as well as online feedback control for eliminating perturbations from the optimal trajectory. In the simulation here, the variational integrator as a variant of a structure-preserving integration scheme is used. A forward rectangular rule is used to approximate the action in one time interval via a discrete Lagrangian $L_d(q_k, q_{k+1}) \approx \int_{t_k}^{t_{k+1}} L(q(s), \dot{q}(s))\mathrm{d}s$ with configuration sequence $q_k \approx q(t_k)$ for $k = 0, \ldots, N$. The configuration $q(t)$ is approximated by a linear polynomial and the velocity by finite differences. Applying a discrete variational principle $\delta S_d(\{q_k\}_{k=0}^N) = 0$, see [1], and an approximation of the virtual work $F_d^{\pm}(q_k, q_{k+1}, u_k)$ with control sequence $\{u_k\}_{k=0}^{N-1}$, the Lagrange-d'Alembert principle yields a discrete Euler-Lagrange equation in a "position-momentum form that only depends on the current and future time steps" [2]. Part of the virtual work is the discretisation of a pulsed disturbance force $F_z(t)$, see [5], acting at time node $t' \in [t_k, t_{k+1})$ and being defined as $F_z(t) = F_{t'}\delta_\epsilon(t - t')$. To compute the desired trajectory, initial and final conditions on the configuration and conjugate momentum, together with the discrete equations in minimal coordinates, serve as non-linear equality constraints for the minimisation of a given objective functional. Applying the DMOC (discrete mechanics and optimal control [3]) algorithm, an optimal trajectory and according control input is calculated. The DMOC solution serves as desired trajectory also for formulation in redundant and nullspace coordinates, their movement is forced to the manifold by using holonomic constraints $g(q(t)) = 0$, $G(q) = \frac{\partial g(q)}{\partial q}$ and a nullspace matrix $P(q)$ with $P^T(q) \cdot G^T(q) = 0$.

Riccati-controller Even when knowing an optimal trajectory $x_{opt} = \begin{bmatrix} q_{opt} & p_{opt} \end{bmatrix}^T$ of a system, in reality the mechanical system will not follow the predefined path because of several perturbations. The correction of these are done by feedback controllers. The key issue is to add an additional control $u_{R,k}$ to the optimal control input $u_k = u_{opt,k} + u_{R,k}$. Here, $u_{R,k}$ is calculated by a linear feedback multiplication of a feedback matrix K_k with e_{x_k}, i.e. $u_{R,k} = K_k e_{x_k}$, with the error $e_{x_k} = x_{opt,k} - x_k$ being the difference between the desired state x_{opt} and the "measured" state x. The resulting block structure is shown in Figure 1.
In the context of the optimal control approach, the Riccati feedback controller is commonly used to minimise a cost-function $V = V_{pen} + V_{eff} = \sum_{k=0}^{N} e_{x_k}^T Q_k e_{x_k} + \sum_{k=0}^{N-1} u_{R,k}^T R_k u_{R,k}$ with (semi-)positive definite weighting matrices Q_k and R_k. After linearising the system to $\delta x_{k+1} = A_k \delta x_k + B_k \delta u_k$, the discrete Riccati equation for non-constant A_k and B_k is applied [6]. Equation (1) is evaluated backwards in time, the initial value is $P_N = Q_N$. After that, the matrix K_k as defined in (2) and the optimal additional control input u_R are calculated.

$$P_k = A_k^T P_{k+1} A_k - A_k^T P_{k+1} B_k (B_k^T P_{k+1} B_k + R_k)^{-1} B_k^T P_{k+1} A_k + Q_k \tag{1}$$

$$K_k = (B_k^T P_{k+1} B_k + R_k)^{-1} B_k^T P_{k+1} A_k \tag{2}$$

Numerical results The described algorithm is applied to several full- and under-actuated systems, for example the under-actuated double pendulum on a cart (cf. Figure 2). The comparison of the Riccati-control algorithm with different coordinate choices, i.e. minimal, redundant, and nullspace coordinates, is done for an optimal upswing from $\theta_1^0 = \theta_2^0 = \pi$ to $\theta_1^N = \theta_2^N = 0$ with $x_0^0 = x_0^N = 0$

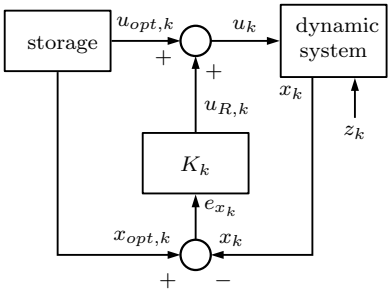

Figure 1: General feedback control

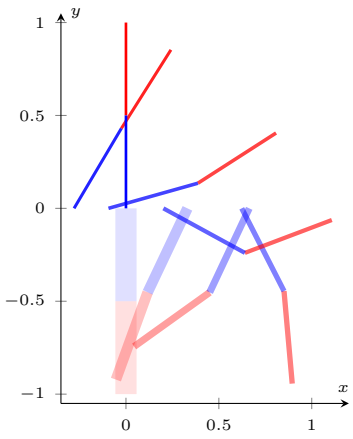

Figure 2: Optimal reference upswing

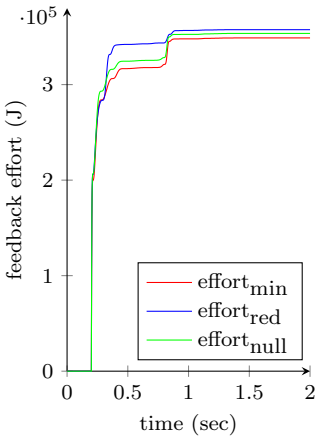

Figure 3: Control effort

calculated in DMOC. The result for a simulation time of $T = 2$s and time step $\Delta t = 0.002$s is plotted in Figure 2. The blue (red) line represents the first (second) pendulum. Stepping forward in time, the lines become thinner and richer in contrast.
At time $t' = 0.2$s, a perturbation with the value $p_z = \begin{bmatrix}0.01\text{Ns} & 0.01\text{Nms} & 0.1\text{Nms}\end{bmatrix}^T$ acts on the system. The controlled trajectories of all three implementations are very similar to each other. In Figure 3, the control effort V_{eff} is plotted for all three coordinate choices. Beginning at $t = t'$, all graphs are strictly increasing as being a sum of positive terms, the gradient corresponds to the control forces. The absolute values differ between all three coordinate choices, but an adequate qualitative behaviour is ensured as cost increases and force peaks occur at the same time for all three cases. After $t = 1.0s$, the perturbation is eliminated.
In summary, we have implemented a Riccati feedback controller for constrained variational integrators. Both the optimal control problem and the Riccati controller are based on the same structure preserving discrete equations of motion. With this approach, a stable handling of highly-nonlinear systems is assured. The feedback control effort reveals that all three coordinate parametrisations only differ slightly. Thus, different choices of coordinates can be used in the feedback control and in the optimal control problem, which might be useful in practice.

References

[1] S. Leyendecker, J. E. Marsden, and M. Ortiz. *Variational integrators for constrained dynamical systems.* ZAMM **88**(9), 677–708 (2008).

[2] E. Johnson, J. Schultz, and T. D. Murphey. *Structured linearization of discrete mechanical systems for analysis and optimal control*, IEEE Transactions on Automation Science and Engineering **12**, 140–152 (2015).

[3] S. Ober-Blöbaum, O. Junge, and J. E. Marsden. *Discrete mechanics and optimal control: An analysis.* ESAIM: COCV **17**(2), 322–352 (2011).

[4] D. Glaas, S. Leyendecker. *Variational integrator for constrained mechanical systems with pulsed disturbances and optimal feedback control.* PAMM **17**(1) 149-150 (2017).

[5] W. Zhao, D. Glaas, and S. Leyendecker, *Variationaler Integrator für geregelte mechanische Systeme mit Zwangsbedingungen und impulsartigen Störungen.* Project thesis, FAU (2017).

[6] B. D. O. Anderson and J. B. Moore. *Optimal Control: Linear Quadratic Methods.* (Prentice-Hall, Inc., 1990).

Numerical convergence analysis of higher order multi-symplectic Lie-group variational integrators for geometrically exact beam dynamics

Thomas Leitz, Sigrid Leyendecker

Multi-symplectic variational integrators are derived by discretizing the action functional of a given dynamical system and applying the discrete Hamilton's principle. This results in the discrete Euler-Lagrange equations, which represent the integrator. In general, they are a non-linear system of equations, which can be solved using e.g. a Newton-Raphson scheme.
In geometrically exact beam dynamics, the deformation map is defined on a two-dimensional space time, where space represents the arc length parameter. The cross sections of the beam are assumed to be rigid. The configuration space is the euclidean space, i.e. the cross sections along the beam have six degrees of freedom – three for the position and three for their orientation.
The discretization of the action functional is done by first discretizing the two-dimensional space time into a regular grid, called the main grid, with $A-1$ elements in space and $J-1$ elements in time. Each space time element of the main grid is further discretized into a regular subgrid with K elements in space and L elements in time.
With the Lagrangian density $\mathcal{L}:[0,T]\times[0,L]\to\mathbb{R}$, the discrete Lagrangian is an approximation of the action functional of one space time element $\mathcal{L}_a^j \approx \int_{s_a}^{s_{a+1}}\int_{t^j}^{t^{j+1}} \mathcal{L}\left(q\left(s,t\right),\partial_t q\left(s,t\right),\partial_s q\left(s,t\right)\right)\mathrm{d}t\mathrm{d}s$ and the discrete action is therefore the sum over all discrete Lagrangians $S_d=\sum_{j=0}^{J-1}\sum_{a=0}^{A-1}\mathcal{L}_a^j$.

Parameterization and interpolation We parameterize the euclidean space by using unit dual quaternions which are defined as $\tilde{\mathbb{H}}^1=\left\{p_r+\varepsilon p_\varepsilon \,|\, p_r,p_\varepsilon\in\mathbb{H},\langle p_r,p_r\rangle=1,\langle p_r,p_\varepsilon\rangle=0,\varepsilon^2=0\right\}$. Every unit dual quaternion can be written as $\tilde{p}=p+\frac{\varepsilon}{2}xp\in\tilde{\mathbb{H}}^1$, where the orientation is encoded in the unit quaternion p and the position is represented by the purely imaginary quaternion x. The interpolation over $(K+1)(L+1)$ unit dual quaternions $\tilde{p}_k$ is done by building the weighted sum and subsequently normalizing, i.e. $\tilde{p}\left(s,t\right)=\frac{\tilde{P}}{\|\tilde{P}\|}$ with $\tilde{P}=\sum_{k=0}^{K}\sum_{l=0}^{L}W_k^l\left(s,t\right)\tilde{p}_k=P_r+\varepsilon P_\varepsilon$, where s and t are the space and time parameter, respectively. This interpolation method avoids shear locking of the beam.

Discrete Euler-Lagrange equations The integral of the discrete Lagrangian is approximated using the interpolation defined above and choosing a suitable quadrature rule. The Lie-group structure preserving variation of a funciton $f:\tilde{\mathbb{H}}^1\to\mathbb{R}$ is defined using the exponential map i.e. $\delta f\left(\tilde{p}\right)=\frac{\mathrm{d}}{\mathrm{d}\epsilon}\big|_{\epsilon=0} f\left(\tilde{p}\exp\left(\epsilon\tilde{\eta}\right)\right)$. With that in mind, the discrete Hamilton's principle results in the discrete Euler-Lagrange equations. These are solved using a Newton-Raphson scheme with iterative reparametrization involving the Cayley map for unit dual quaternions in order to avoid constraint functions.

Results The simulation of a beam was carried out with different time steps Δt, different space steps Δs, as well as different polynomial degrees in time K and space L. Figures 1a and 1b show the convergence of the integrator for time and space refinement with constant polynomial orders L and K. The errors are of order $\mathcal{O}\left(\Delta t^{2L}\right)$ and $\mathcal{O}\left(\Delta s^{2K}\right)$, respectively.
Figures 1c and 1d show the convergence of the integrator for K and L polynomial refinement with constant time and space steps Δt and Δs. The errors are of order $\mathcal{O}\left(\Gamma_l^L\right)$ and $\mathcal{O}\left(\Gamma_k^K\right)$, respectively.

Conclusion We derived a multisymplectic Lie-group variational integrator of arbitrary order based on unit dual quaternion interpolation for the simulation of geometrically exact beam dynamics. The order of the integrator depends solely on the polynomial degree of the interpolation, paired with an appropriate quadrature rule used to compute the discrete Lagrangian.

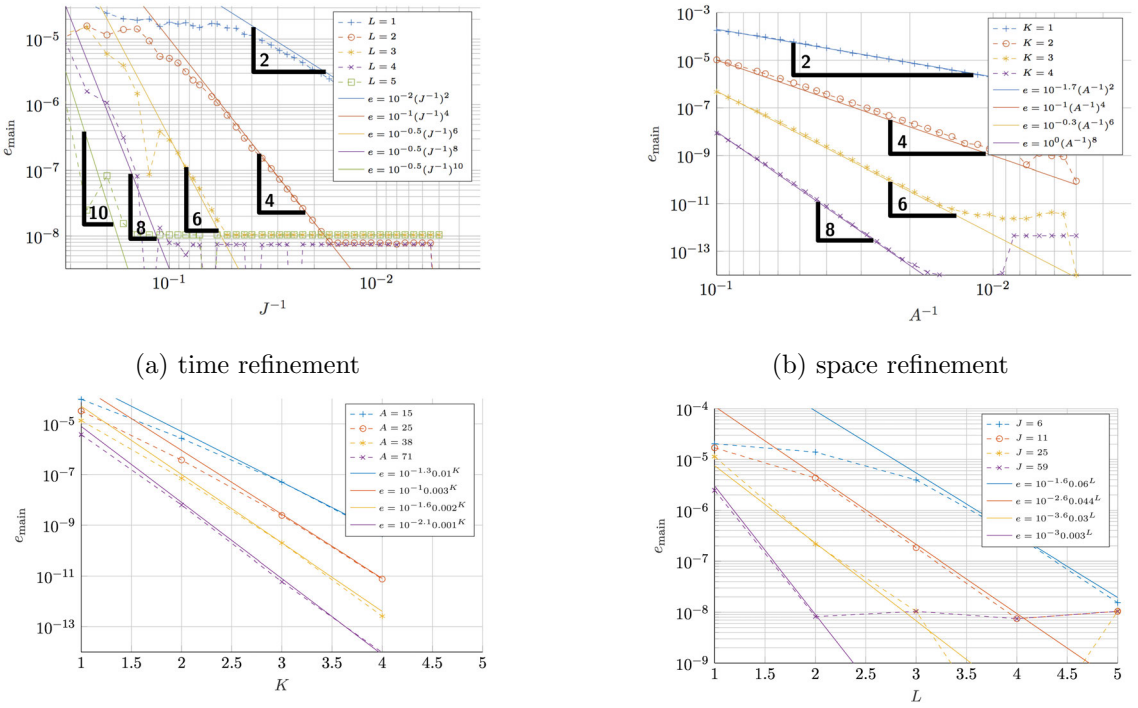

(a) time refinement

(b) space refinement

(c) K refinement

(d) L refinement

Figure 1: Convergence plots

References

[1] François Demoures, François Gay-Balmaz, Marin Kobilarov, and Tudor S. Ratiu. Multisymplectic lie group variational integrator for a geometrically exact beam in r3. *Communications in Nonlinear Science and Numerical Simulation*, 19(10):3492–3512, 2014.

[2] James Hall and Melvin Leok. Lie group spectral variational integrators. *Foundations of Computational Mathematics*, pages 1–59, 2015.

[3] Thomas Leitz and Sigrid Leyendecker. Towards higher order multi-symplectic lie-group variational integrators for geometrically exact beam dynamics – avoidance of shear locking. In *8th ECCOMAS Thematic conference on MULTIBODY DYNAMICS*, 2017.

[4] J. Simo. A finite strain beam formulation. the three-dimensional dynamic problem. part i. *Computer Methods in Applied Mechanics and Engineering*, 49(1):55–70, 1985.

Optimal control of a slot car racer using a discrete variational principle

Johann Penner, Tristan Schlögl, Sigrid Leyendecker

In order to describe and control the behavior of a slot car racer, a suitable simulation model is required. The functional principle of this electric vehicle merges mechanics and electronics and can generally be described in terms of differential equations by physical laws, such as Faraday's law, Coulomb's law, Kirchhoff's law and d'Alembert's principle. These second-order differential equations can be obtained via a variational principle based on an energy functional [1, 2]. The optimal control simulation method in this work is a direct discretisation technique for mechanical systems – that has been extended for mechatronical systems – known as DMOC [5] and is based on a discrete variational principle. The derivation of the system dynamics with discrete variational calculus requires to formulate the electrical, magnetic and mechanical energy of the system and to apply the discrete Lagrange-d'Alembert principle. This is less common in electrical engineering but leads to a structure preserving time stepping scheme which serves as equality constraints for the nonlinear programming problem, resulting from the discretisation of the optimal control problem by DMOC [3, 4, 5, 6]. The computed optimal voltage profiles are embedded into an experimental setup for a slot car racer with an underlying camera tracking system which allows to correct the vehicle towards the desired state via a computer.

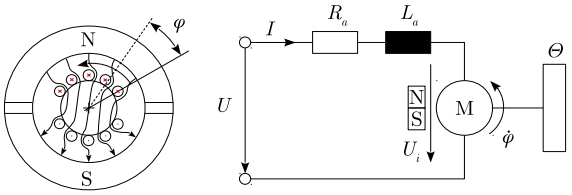

Figure 1: Idealized model of a DC motor

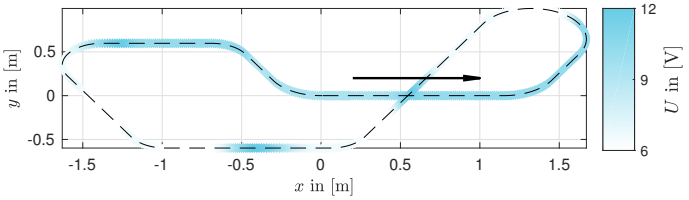

Figure 2: Driving voltages versus track position

According to the discrete variational principle, we choose a time grid $\Delta t = \{t_0, t_1, ..., t_N\}$ for the discrete path $\mathbf{q}_d = \{\mathbf{q}_n\}_{n=0}^{N}$ with step size $h \in \mathbb{R}$ and the midpoint rule for the approximation of the integrals in the Lagrange-d'Alembert principle. The discrete forced Euler-Lagrange equations for $n = 1, ..., N-1$

$$D_1 L_d(\mathbf{q}_n, \mathbf{q}_{n+1}) + D_2 L_d(\mathbf{q}_{n-1}, \mathbf{q}_n) + \mathbf{f}_d^-(\mathbf{q}_n, \mathbf{q}_{n+1}, \mathbf{u}_n) + \mathbf{f}_d^+(\mathbf{q}_{n-1}, \mathbf{q}_n, \mathbf{u}_n) = \mathbf{0} \tag{1}$$

follow from the discrete Lagrange-d'Alembert principle, where $D_\bullet L_d$ is the slot derivative with respect to the $\bullet$-th argument and $\mathbf{f}_d$ are the discrete forces. The discrete momenta are given by the discrete Legendre transformation as $\mathbf{p}_n^- = -D_1 L_d(\mathbf{q}_n, \mathbf{q}_{n+1}) - \mathbf{f}_d^-(\mathbf{q}_n, \mathbf{q}_{n+1}, \mathbf{u}_n)$ and $\mathbf{p}_n^+ = D_2 L_d(\mathbf{q}_{n-1}, \mathbf{q}_n) + \mathbf{f}_d^+(\mathbf{q}_{n-1}, \mathbf{q}_n, \mathbf{u}_n)$, where $\mathbf{p}_0^-$ is used for the first time step. The DMOC method deals with the problem of finding the discrete control forces $\mathbf{u}_d = \{\mathbf{u}_n\}_{n=0}^{N-1}$ with respect to a given system – in terms of discrete Euler-Lagrange equations – such that a certain discrete objective function J_d or, respectively, a discrete cost function C_d is minimized, i.e.

$$\min_{\mathbf{q}_d, \mathbf{u}_d} J_d(\mathbf{q}_d, \mathbf{u}_d, h) = \min_{\mathbf{q}_d, \mathbf{u}_d, h} \sum_{n=0}^{N-1} C_d(\mathbf{q}_n, \mathbf{q}_{n+1}, \mathbf{u}_n, h) \qquad \text{subject to } \begin{array}{l} \cdot \text{equation (1)} \\ \cdot \text{initial and final conditions} \\ \cdot \text{additional constraints} \end{array} \tag{2}$$

Assuming that the considered slot car has an idealized DC motor (see Figure 1), the discrete path $\mathbf{q}_d = \left\{[Q_n, \varphi_n]^T\right\}_{n=0}^{N}$ comprises the total amount of moving electric charge Q_n, that has passed any point of the motor windings – where φ_n denotes the rotation angle – at each time step. The discrete control parameter $\mathbf{u}_d = \{U_n\}_{n=0}^{N-1}$ is reduced to a sequence of driving voltages U_n and the current I_n is defined as flow electric charges over time. In the case of a DC motor, the Lagrangian consists only of the magnetic-field co-energy and the mechanical energy of the motor shaft, such that the discrete Lagrangian reads

$$L_d(\mathbf{q}_n, \mathbf{q}_{n+1}) = \frac{h}{2}\left\{\frac{L_a}{h^2}\left(Q_{n+1} - Q_n\right)^2 + \frac{K}{2h}\left(\varphi_{n+1} + \varphi_n\right)\left(Q_{n+1} - Q_n\right) + \frac{\theta}{h^2}\left(\varphi_{n+1} - \varphi_n\right)^2\right\} \tag{3}$$

where θ denotes the inertia of the rigid motor shaft, L_a is the inductance of the windings and K is a machine constant. The discrete forces (with arguments as in equation (1)) are given by

$$\mathbf{f}_d^- = \begin{bmatrix} h\,U_n + \frac{R_a}{2}\left(Q_{n+1} - Q_n\right) \\ \frac{h}{4}\left(M_{n+1} + M_n\right) \end{bmatrix} \qquad \mathbf{f}_d^+ = \begin{bmatrix} h\,U_n - \frac{R_a}{2}\left(Q_n - Q_{n-1}\right) \\ \frac{h}{4}\left(M_n + M_{n-1}\right) \end{bmatrix} \tag{4}$$

with the external friction torque $M_n = \frac{r}{i}(F_c \tanh(v_n) + \tau_v v_n)$ and the power dissipation $-R_a I_n$. Herein, a continuous velocity-based friction model – with sliding friction F_c and the viscous friction parameter τ_v – approximates the friction force acting of the slot car. The current is written as a finite difference $I_n = \frac{(Q_{n+1}-Q_n)}{h}$. Under the assumption of a rolling wheel with radius r and the gear ratio of the slot car i, we can compute the velocity $v_n = \frac{r}{i}\frac{\varphi_{n+1}-\varphi_n}{h}$ and the covered distance $s_{n+1} = s_n + v_n h$ of the vehicle. For this electromechanically coupled system the general momenta $\mathbf{p}_n = [p_n^Q, p_n^\varphi]^T$ consist of the flux linkage p_n^Q and the mechanical momentum p_n^φ at each time step. The time-minimal path can be modeled using different cost functions, where the problem of minimizing the lap time is equivalent to maximizing the velocity – or momentum – for each lap. Within this work, we concentrate on a combined objective function J_d that minimizes the lap time – which corresponds to the sum of time steps – together with the change of driving voltages.

$$J_d(\mathbf{q}_d, \mathbf{u}_d, h) = c_u \sum_{n=0}^{N-1} \left(\frac{U_{n+1} - U_n}{h} \right)^2 + \sum_{n=0}^{N} h \tag{5}$$

Herein, the weighting factor $c_u \in \mathbb{R}$ ensures that the influence of lap time and driving voltages on the cost function are of the same order of magnitude. Furthermore, we can substitute the sum of time steps J_t with the negative sum of the quadratic velocities J_v or the negative sum of the quadratic momenta J_p.

$$J_t(h) = \sum_{n=0}^{N} h \qquad J_v(\mathbf{q}_d, h) = -\sum_{n=0}^{N-1} \left(\frac{s_{n+1} - s_n}{h} \right)^2 \qquad J_p(\mathbf{q}_d, h) = -\sum_{n=0}^{N-1} \left(p_n^{\varphi-} \right)^2 \tag{6}$$

The calculated optimal driving voltages for the time minimal path respecting the maximal admissible velocity for the race track are shown in Figure 2.

References

[1] U. Diemar, and E. Kallenbach, VDI-Bericht **1892**, 295–314 (2005).

[2] R. Ortega, A. Loria, P. J. Nicklasson, and H. Sira-Ramirez, Passivity-Based Control of Euler-Lagrange Systems (Springer-Verlag, Berlin, 1998), p. 265.

[3] K. Flaßkamp, S. Ober-Blöbaum, T. Schneider and J. Böcker, 52nd IEEE Conference on Decision and Control, Florence, Italy, CDC, 2013, pp. 7467–7473.

[4] J. E. Marsden, and M. West, Acta Numerica **10**, 357–514 (2001).

[5] S. Ober-Blöbaum, O. Junge, and J. E. Marsden, ESAIM: Control, Optimisation and Calculus of Variations **17**, 322–352 (2011).

[6] S. Ober-Blöbaum, M. Tao, M. Cheng, H. Owhadi, and J. E. Marsden, Journal of Computational Physics **242**, 498–530 (2013).

Optimal control simulations of two finger grasping

Uday D. Phutane, Michael Roller[2] , Sigrid Leyendecker

Introduction Grasping is a basic, though complex human movement performed with the hand through its many degrees of freedom. During grasping, when the hand closes around the object, the multibody system changes from a kinematic tree structure to a closed loop contact problem. To better understand work-related disorders or optimize execution of activities of daily living, an optimal control simulation to perform grasping would be useful. The optimal control problem in this work is solved using the direct transcription method DMOCC (discrete mechanics and optimal control with constraints), see [4], leading to a structure preserving approximation. The contact mechanics is realised using spherical joints, see [3], as opposed to using a penalty potential.

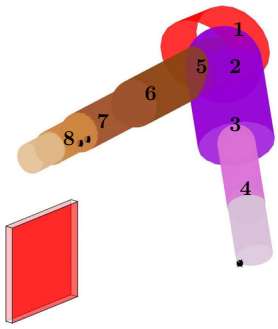

Figure 1: The two finger model with the object to be grasped.

joint	cardan	nino	revolute	fixed
1	✗			
2		✗		
3		✗		
4			✗	
5				✗
6	✗			
7			✗	
8			✗	

Table 1: The table lists the different joints used in the model.

To understand the mechanics of grasping for the complete hand, a simplified two finger model is a good start. The multibody system simulated here is made up of the wrist along with the thumb and index finger, as shown in Figure 1. The model is constituted through different joint descriptions, such as the cardan, nino (non-intersecting, non-orthogonal axes, described in [1]), revolute and fixed joints, as listed in Table 1. Using the multibody formulation described in [2], the model is described with a redundant configuration variable, $\boldsymbol{q}$, with internal constraints m_{int} and external constraints m_{ext}, in effect reducing the system to eleven degrees of freedom. The model is actuated using joint torques. The dynamics of the object, in this case a box, is also taken into account for grasping, which adds another six degrees of freedom for its dynamics.

The grasping movement is composed of a reaching phase (no contact between the fingers and the object) and a grasping phase (closed contacts), see Figure 2. In the first phase, the fingers, described through the open kinematic chains, approach the surfaces of the object to be grasped. The discrete Euler-Lagrange (DEL) equations to describe the dynamics are obtained using the variational principle along with the discrete nullspace matrix $\boldsymbol{P}$, $\boldsymbol{P}^B$, see [2], for the hand and the object, respectively. Additionally, we employ the discrete nodal reparameterisation to further reduce the number of equations of motion for the hand. At time node N_k, the contact is closed through gap functions $\boldsymbol{g}_{c1}$ and the contact points on the object are defined within the surface

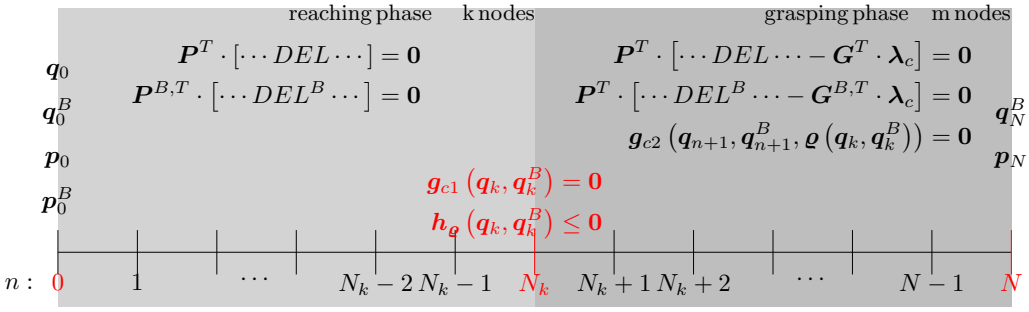

Figure 2: Time grid with dynamical constraints of the optimal control problem.

[2]Fraunhofer Institute for Industrial Mathematics, Kaiserslautern, Germany

limits $\boldsymbol{h_g}$. In the following phase, the contact is maintained through spherical joints $\boldsymbol{g}_{c1}$ forming a closed loop. The DEL equations for this phase get modified to represent the contact forces on the two systems, which are described through the contact constraint Jacobians $\boldsymbol{G}$, $\boldsymbol{G}^B$ and Lagrange multipliers. The duration of the two phases are also obtained as a result of the optimal control problem. This constitutes a hybrid dynamical system with a known switching sequence with unknown switching times.

Example We execute an optimal control simulation to perform a lateral pinch (like holding a key), between the thumb pulp (one contact point) and radial side of the medial phalange (two contact points), as shown in Figure 3. The boundary conditions are with fixed initial configurations for the hand and the object and to perform a rest-to-rest manoeuvre. The objective function minimised is a linear combination of the sum of the squares of joint torques and the rate of change of the joint torques.

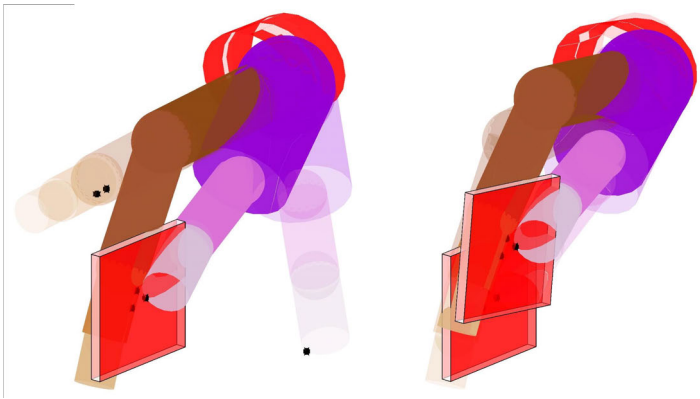

Figure 3: The progression of the grasp manoeuvre from initial position to contact closing with the finger-fixed contact points ($*$) on the object surfaces and lifting it to the final position (from left to right). The contact is closed at time node $N_k = 5$ and have $N_m = 4$ time nodes to perform the grasping action.

References

[1] U. Phutane, M. Roller, S. Björkenstam, J. Linn and S. Leyendecker. Kinematic validation of a human thumb model. ECCOMAS Thematic Conference on Multibody Dynamics, 2017.

[2] P. Betsch, and S. Leyendecker. The discrete null space method for the energy consistent integration of constrained mechanical systems. Part II: Multibody dynamics. Int. J. Numer. Meth. Engng., Vol. 67, pp. 499-552, 2006.

[3] M.W. Koch, and S. Leyendecker. Structure Preserving Simulation of Monopedal Jumping. Archive of Mechanical Engineering, DOI 10.2478/meceng-2013-0008, Vol. LX, pp. 127-146, 2013.

[4] S. Leyendecker, S. Ober-Blöbaum, J.E. Marsden, and M. Ortiz. Discrete mechanics and optimal control for constrained systems. Optimal Control Applications and Methods, 31:505-528, 2010.

A polarisation based approach to model strain dependent electrostatic pressure of dielectric elastomer actuators

Tristan Schlögl, Sigrid Leyendecker

Introduction Dielectric elastomer actuators (DEAs) are composed of an elastic dielectric material that is sandwiched between two compliant electrodes, as illustrated in Figure 1. When the electrodes are charged by applying an electric potential, charges with opposite signs attract each other, leading to a contractive force also known as electrostatic pressure [1]. When several DEA cells are stacked on top of each other, resulting in a pile-up configuration, the electrostatic pressure provides macroscopically useful displacements [2]. Stacked DEAs are also referred to as artificial muscles, because they bear analogy to the behaviour of human muscles in terms of contracting in length direction when stimulated.

The behaviour of artificial muscles can generally be described by considering coupling forces between the applied electric field (whose distribution has to fulfil the Maxwell equations for electrostatics) and the deformation gradient (that is characterised by the mechanical momentum balance) as shown by Dorfmann et. al. in 2005 [3]. In 2007, Vu et. al. [4] solved the equations proposed by Dorfmann for arbitrary geometries in the static case, numerically simulated using the finite element method. The static formulation of Vu was extended by inertia terms that allow for dynamic motion and structure preserving time integration by Schlögl et. al. in 2016 [5]. Even though these models provide a powerful tool to solve electromechanically coupled and dynamic problems of arbitrary geometry, the computational cost is quite demanding. To find solutions for complex control problems where a multibody system is actuated by several muscles at the same time as in [6], it is necessary to make use of lumped parameter models that reduce the computational cost.

Common modelling approach The following derivation of the electrostatic pressure is inspired by [7], where the interaction between electrical and mechanical quantities is examined via the principle of virtual work. As illustrated in Figure 1, the two compliant electrodes with surface area $A(z)$ enclose the dielectric with permittivity ε_r. When a constant voltage U is applied, the electrodes get charged with the amount $Q(z)$, depending on the distance between the electrodes z. The contractive force between the capacitor plates is assumed to be acting in z-direction only, with its z-component given by $F(z)$. All quantities are either constant or depend only on the distance z, hence the dimension of the lumped parameter model is reduced to one degree of freedom. Moreover, all quantities are assumed to be quasi-static, neglecting any time dependent effects.

The unknown force $F(z)$ can be calculated by applying the principle of virtual work

$$\delta W^{\text{ext}}(z) = \delta W^{\text{elec}}(z) + \delta W^{\text{mech}}(z), \tag{1}$$

requiring an infinitesimal amount of energy brought into the system via the external power supply $\delta W^{\text{ext}}(z)$ to be identical with the change of energy stored in the system, separated into electrical energy $\delta W^{\text{elec}}(z)$ and mechanical energy $\delta W^{\text{mech}}(z)$. For the capacity of a parallel plate capacitor and constant volume $V = A(z)\, z$ (due to the incompressibility of the dielectric and compliant electrodes), the contractive force is given as

$$F(z) = \varepsilon_0 \varepsilon_r A(z) \frac{U^2}{z^2}, \tag{2}$$

with ε_0 being the vacuum permittivity.

New polarisation based model Using the parallel plate capacitor formula in the previous section implicitly assumes linear polarisation within the dielectrics. Evaluating the principle of virtual work for arbitrary polarisation $P(z)$, the contractive force

$$F = A \left(\varepsilon_0 E^2 - \frac{1}{2} \partial_z P E z + \frac{1}{2} P E \right) \tag{3}$$

is obtained, where the electric field is given by $E = U/z$. The polarisation P can be derived from an electromechanically coupled, hyperelastic material approach as shown in [3], such that the contractive force (3) becomes

$$F = A E^2 \left(\varepsilon_0 - 2c_1 - 4\lambda^{-2} c_2 \right), \tag{4}$$

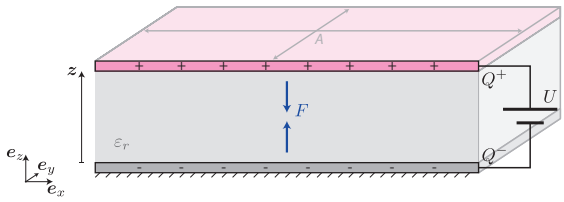

Figure 1: Lumped parameter model of DEA cell.

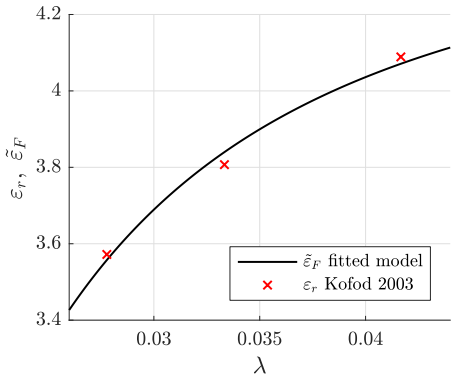

Figure 2: Relative permittivity measured by Kofod [8] and new polarisation based model fit.

where c_1 and c_2 are material parameters and $\lambda = z/z_0$.

Figure 2 shows how the new model compares to measurement data. The material parameters are fitted using a non-linear least squares trust-region algorithm provided by MATLAB's curve fitting toolbox. The measured relative permittivity is compared to the stretch dependent equivalent $\tilde{\varepsilon}_F$ of the polarisation based model. Note that in the wide spread model first mentioned in [1], the relative permittivity is a constant quantity that does not cover any stretch dependency at all.

References

[1] R.E. Pelrine, R.D. Kornbluh, and J.P. Joseph. Sens. Actuators, A, Vol. 64, pp. 77-85, 1998.

[2] G. Kovacs, L. Düring, S. Michel, and G. Terrasi. Sens. Actuators, A, Vol. 155, pp. 299-307, 2009.

[3] A. Dorfmann and R.W. Ogden. Acta Mech, Vol. 174, pp. 167-183, 2005.

[4] D.K. Vu, P. Steinmann, and G. Possart. Int. J. Numer. Meth. Engng, Vol. 70, No. 6, pp. 685-705, 2007.

[5] T. Schlögl and S. Leyendecker. Comput. Methods Appl. Mech. Engrg., Vol. 299, pp. 421-439, 2016.

[6] T. Schlögl and S. Leyendecker. Proceedings of the ASME 2016 Conference SMASIS, 2016.

[7] M. Wissler and E. Mazza. Sens. Actuators, A, Vol. 138, pp. 384-393, 2007.

[8] G. Kofod, P. Sommer-Larsen, R. Kornbluh, and R. Pelrine. J. Intell. Mater. Syst. Struct., Vol. 14, No. 12, pp. 787-793, 2003.

Variational integrators of mixed order for constrained multirate systems

Theresa Wenger, Sina Ober-Blöbaum[3], Sigrid Leyendecker

The considered constrained multirate systems contain dynamics on different time scales caused by different types of potentials. For the slow motion, a coarse approximation suffices, but to resolve the fast motion, high accuracy is required. To avoid unnecessary computational costs, the idea is to use polynomials of different degrees to approximate the slow and fast dynamics and quadrature formulas of different orders to approximate the different action terms. The Lagrange multiplier theorem is used to introduce constraint forces constraining the motion to the constraint manifold.

Consider an n-dimensional mechanical system, defined on the n-dimensional vector space Q, with time t dependent configuration vector $q(t) \in Q$ and velocity $\dot{q}(t) \in T_{q(t)}Q$. Let the motion be dividable into fast and slow components, such that n^s slow variables $q^s \in Q^s$ and n^f fast variables $q^f \in Q^f$ can be assigned, where $q = (q^s, q^f)^T$, $Q = Q^s \times Q^f$, $n = n^s + n^f$. The Lagrangian $L : TQ \to \mathbb{R}$ is supposed to be separable, reading $L(q, \dot{q}) = T(\dot{q}) - V(q) - W(q^f)$, and consists of a potential with different parts that lead to strongly varying dynamics, split into a slow potential V and a fast potential W accordingly. We assume that $V = V(q)$ depends on the complete configuration and $W = W(q^f)$ only on the fast configuration. Let the system be constrained by the vector valued function $g(q) = 0 \in \mathbb{R}^m$ to the $(n-m)$-dimensional submanifold $C = g^{-1}(0)$. The constraints that depend only on the slow configuration are marked as $g^s = g^s(q^s)$. The term $g^{sf} = g^{sf}(q^s, q^f)$ includes the constraints that depend on the complete configuration or the fast configuration only. It is not necessary to distinguish between the dependence on the complete or the fast configuration as the corresponding constraints are treated identically in the discrete case. The Lagrangian is augmented by $g(q) \cdot \lambda$, where $\lambda(t) \in \mathbb{R}^m$ is the Lagrange-multiplier. The augmented Lagrangian $\bar{L} : TQ \times \mathbb{R}^m$ is then written in the form $\bar{L}(q, \dot{q}, \lambda) = L(q, \dot{q}) - g^s(q^s) \cdot \lambda^s - g^{sf}(q^s, q^f) \cdot \lambda^f$, with $g(q) = (g^s(q^s), g^{sf}(q^s, q^f))^T$ and $\lambda = (\lambda^s, \lambda^f)^T$, $\lambda^s \in \mathbb{R}^{m^s}$, $\lambda^f \in \mathbb{R}^{m^f}$, $m^s + m^f = m$. The time integral of the augmented Lagrangian over $[0, T]$ yields the augmented action $\bar{S} : \mathcal{C}(Q \times \mathbb{R}^m) \to \mathbb{R}$, with fixed endpoints $q_0, q_N \in C$ and $\mathcal{C}(\mathbb{R}^m) = \mathcal{C}([0, T], \mathbb{R}^m)$ being the space of curves $\lambda : [0, T] \to \mathbb{R}^m$ with no boundary conditions. For the construction of the variational integrators, the action is approximated and Hamilton's principle is applied, see e.g. [1]. The entire time interval $[0, T]$ is divided into N subintervals $[kh, (k+1)h]$, $k = 0, \ldots, N-1$ of the same length h. Finite-dimensional function spaces Π^a are chosen to approximate the continuous curves on each of the subintervals, where Π^a denotes the space of polynomials of degree a. In particular, the polynomial $q^s_{d,k} : [0, h] \to Q^s$, $q^s_{d,k} \in \Pi^{ps}$ (resp. $q^f_{d,k} : [0, h] \to Q^f$, $q^f_{d,k} \in \Pi^{pf}$) is an approximation for $q^s : [kh, (k+1)h] \to Q^s$ (resp. $q^f : [kh, (k+1)h] \to Q^f$). The polynomial $\lambda^s_{d,k} : [0, h] \to \mathbb{R}^{m^s}$, $\lambda^s_{d,k} \in \Pi^{ws}$ (resp. $\lambda^f_{d,k} : [0, h] \to \mathbb{R}^{m^f}$, $\lambda^f_{d,k} \in \Pi^{wf}$) is an approximation for $\lambda^s : [kh, (k+1)h] \to \mathbb{R}^{m^s}$ (resp. $\lambda^f : [kh, (k+1)h] \to \mathbb{R}^{m^f}$). A continuous approximation on $[0, T]$ is ensured by $q^s_{d,k}(h) = q^s_{d,k+1}(0)$, $q^f_{d,k}(h) = q^f_{d,k+1}(0)$, $\lambda^s_{d,k}(h) = \lambda^s_{d,k+1}(0)$ and $\lambda^f_{d,k}(h) = \lambda^f_{d,k+1}(0)$, $k = 0, \ldots, N-1$. Furthermore, different quadrature rules are used to approximate the contributions of the action on each time interval. The discrete augmented Lagrangian $\bar{L}_{d,k}(q_{d,k}, \dot{q}_{d,k}, \lambda_{d,k}) = L_{d,k} - g_{d,k}$, with $L_{d,k}(q_{d,k}, \dot{q}_{d,k}) \approx \int_{kh}^{(k+1)h} L(q, \dot{q})\, dt$ and $g_{d,k}(q_{d,k}, \lambda_{d,k}) \approx \int_{kh}^{(k+1)h} g(q) \cdot \lambda\, dt$, reads

$$L_{d,k}(q_{d,k}, \dot{q}_{d,k}) = h \sum_{i=1}^{r^t} b_i^t T(\dot{q}^s_{d,k}(c_i^t h), \dot{q}^f_{d,k}(c_i^t h)) - h \sum_{i=1}^{r^v} b_i^v V(q^s_{d,k}(c_i^v h), q^f_{d,k}(c_i^v h)) - h \sum_{i=1}^{r^w} b_i^w W(q^f_{d,k}(c_i^w h))$$

$$g_{d,k}(q_{d,k}, \lambda_{d,k}) = h \sum_{i=0}^{z^s} e_i^s g^s(q^s_{d,k}(f_i^s h)) \cdot \lambda^s_{d,k}(f_i^s h) + h \sum_{i=0}^{z^f} e_i^f g^{sf}(q^s_{d,k}(f_i^f h), q^f_{d,k}(f_i^f h)) \cdot \lambda^f_{d,k}(f_i^f h)$$

[3]Department of Engineering Science, University of Oxford, England

with $q_{d,k} = (q^s_{d,k}, q^f_{d,k})$, $\dot{q}_{d,k} = (\dot{q}^s_{d,k}, \dot{q}^f_{d,k})$, $\lambda_{d,k} = (\lambda^s_{d,k}, \lambda^f_{d,k})$ and quadrature nodes $c^j_i \in [0,1]$ (resp. $f^l_i \in [0,1]$) and associated weights b^j_i, $j = t, v, w$, c.f. [3] (resp. e^l_i, $l = s, f$). For the calculation of $g_{d,k}$, restrictions are given that ensure the solvability of the corresponding discrete Euler-Lagrange equations (DEL) and stiff accuracy, i.e. avoidance of the discrete solution to drift off C at the nodes $q^s_{d,k}(0)$ and $q^f_{d,k}(0)$, $k = 1, \ldots, N-1$. First, all quadrature nodes f^s_i (resp. f^f_i) have to be part of the time control points $0 = \tilde{d}^s_0 < \ldots < \tilde{d}^s_{ws} = 1$ of λ^s_d (resp. of the time control points $0 = \tilde{d}^f_0 < \ldots < \tilde{d}^f_{wf} = 1$ of λ^f_d). As a consequence, the number of unknowns equals the number of equations in one time step. Additionally, $f^s_{z^s} = 1$ and $f^f_{z^f} = 1$ lead to a stiffly accurate integration scheme. The Lobatto quadrature entails this and is used here, yielding the restrictions $ps \geq ws$ and $pf \geq wf$ that guarantee the linear independence of the discrete equations. See [2] for more details.

Computational efficiency The performance of the presented integrators is tested by means of a triple pendulum (TP), see Fig. 1 (left). The position of the masses m_i are described by the vectors $q_i \in \mathbb{R}^3$, $i = 1, 2, 3$. The motion of the big mass m_1 is rather slow compared to that of the small masses m_2 and m_3 that are linked by a very stiff linear spring, yielding a quadratic fast potential $W(q_2, q_3)$. The norm of the gravitation $a = -\frac{1}{8}((q_1 - q_2) \cdot e_3)^4 e_3$ varies with the fourth power, such that the gravitational energy associated with the slow potential $V(q_1, q_2, q_3)$ is highly nonlinear. The constraint $g^s(q_1)$ constrains m_1 to a sphere with radius l_1, while $g^{sf}(q^1, q^2)$ prescribes the distance between m_1 and m_2 to be l_2. One approach to save run-time is to reduce the degree ps of the polynomial q^s_d while keeping a higher degree pf of q^f_d, as the number of unknowns in the DEL then decreases. Furthermore, reducing the order oV of the quadrature formula used to approximate the integral of the slow potential V reduces the number of costly evaluations of the Jacobian $\nabla V(q)$. With the trapezoidal rule, even more run-time can be saved, because the Hessian of the slow potential, used when solving the implicit DEL via an iteration scheme like the Newton-Raphson method, is not needed. Simulating the constrained TP system, run-time savings can be achieved compared to the constrained high order variational integrator $ps = pf = 3$, Gauss-quadrature rule of order 6 for all contributions of the Lagrangian and $ws = ps$, $wf = pf$ (turquoise plus signs), see Fig. 1 (right). The same accuracy (smaller than the Newton tolerance 10^{-8}) is reached by a decreased order oV of 4 (orange stars) in a faster way. Choosing $ps = 2$ together with $oV = 4$ (Gauss, purple circles) or $oV = 2$ (Lobatto, green squares) leads to a slightly reduced accuracy. Thus, for assessing the most efficient integrators the desired accuracy is crucial.

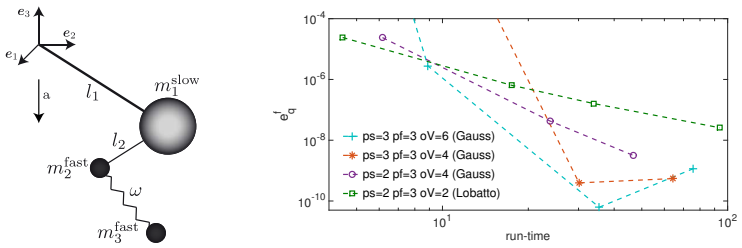

Figure 1: TP (left): Error of fast configuration over run-time (right)

References

[1] J. E. Marsden and M. West, Acta Numerica **10**, 357–514 (2001).

[2] T. Wenger, S. Ober-Blöbaum and S. Leyendecker, Advances in Computational Mathematics **43**, 1163–1195 (2017)

[3] T. Wenger, S. Ober-Blöbaum and S. Leyendecker, ECCOMAS Congress 2016 Proceedings **1**, 1818–1831 (2016).

4 Activities

4.1 Dynamic laboratory

The dynamic laboratory – modeling, simulation and experiment (Praktikum Technische Dynamik) adresses all students of the Technical Faculty of the FAU Erlangen-Nürnberg. The aim of the practical course is to develop mathematical models of fundamental dynamical systems to simulate them numerically and compare the results to measurements on the mechanical system. Here, the students experience both the possibilities and limitations of computer based modeling. The course starts with one central introductory programming task, followed by six experimental setups, including modeling, simulation, and experiment:

- programming training
- beating pendulums
- gyroscope
- ball balancer
- robot arm
- inverse pendulum
- balancing robot

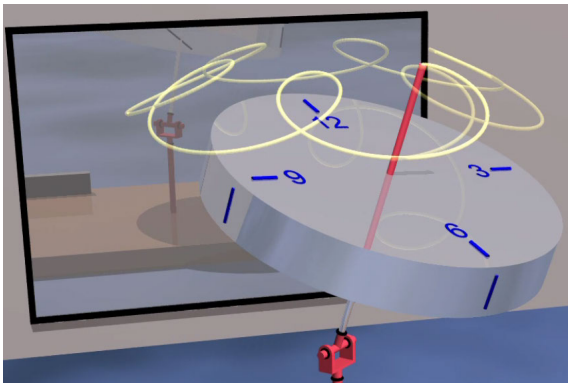

programming training

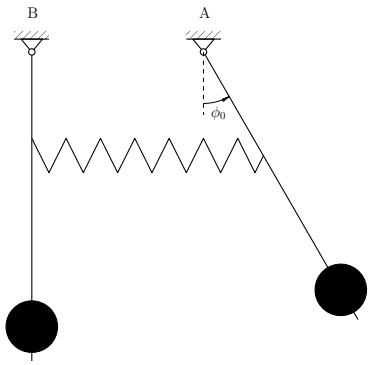

beating pendulums

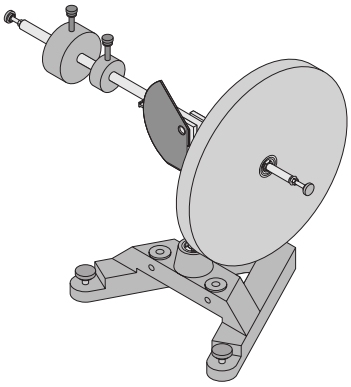

gyroscope

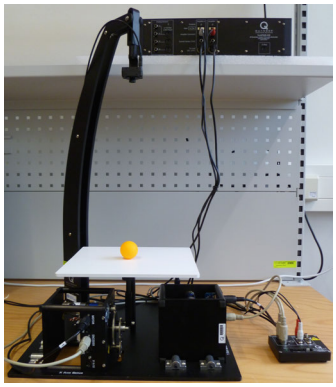

ball balancer

robot arm

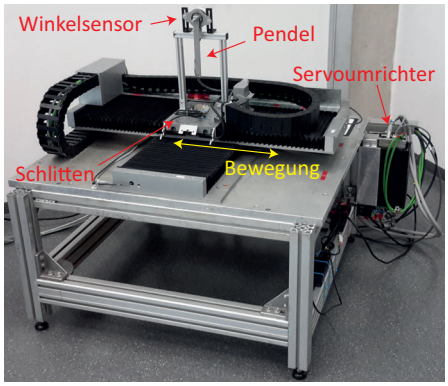

inverse pendulum

balancing robot

Slot car racer The LTD's computer controlled slot car racer has been extended by a powerful industrial camera and a new data acquisition device. The UI-3060CP USB-3 camera from IDS provides excellent image quality, a high refresh rate of 166 fps at 2.4 MP, low input delay and extremely low noise. The PCIe-6321 data acquisition board from National Instruments integrates high-performance analog, digital, and counter/timer functionality into a single device, making it well-suited to control the slot car via a computer. These new components will bring significant improvement to the slot car tracking lag and hence to a control system that allows to correct the vehicle towards the desired state.

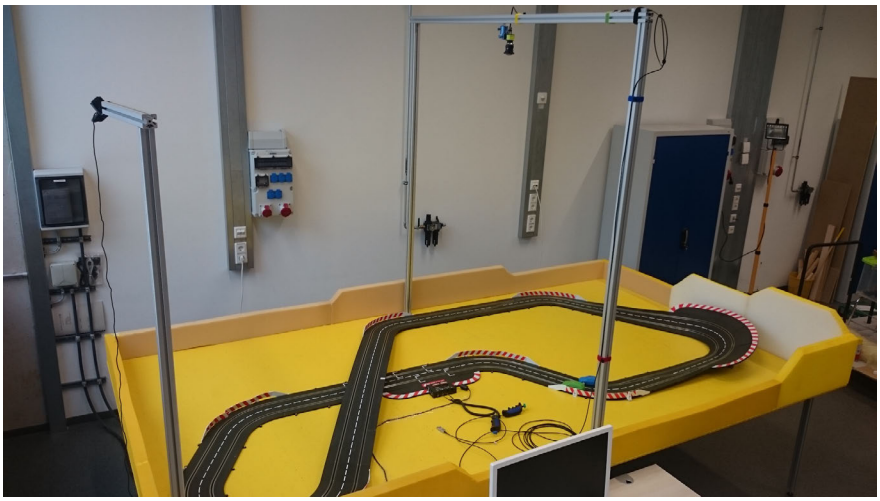

The slot car racer with the new industrial camera

4.2 MATLAB laboratory

The MATLAB laboratory (MATLAB Praktikum) course is organized by the Chair of Applied Dynamics (LTD) in coordination with the Chair of Applied Mechanics (LTM), the Chair for Production Metrology (FMT) and Chair for Engineering Design (KTmfk). The course aims to develop programming skills in MATLAB by numerically solving problems in mechanical engineering. Every participating chair sets up a task to simulate a mathematical model of a physical system which is relevant to the courses and research carried out at the particular chair. For example, the LTD task is to model a Crane and solve its dynamics, the tasks for the LTM and KTmfk chairs concern the design of a bridge (static truss) for stiffness and optimization, and the FMT task discusses the concept of Fourier transformation with respect to the analysis of measurement data.

4.3 Teaching

Wintersemester 2017/2018

Dynamik starrer Körper (MB, ME, WING, IP, BPT, CE, MT)		
Vorlesung		S. Leyendecker, T. Wenger
Übung + Tutorium		T. Bentaleb, D. Budday T. Gail, T. Leitz J. Penner, U. Phutane
Mehrkörperdynamik (MB, ME, WING, TM, BPT, MT)		
Vorlesung + Übung		T. Wenger
entfallen im WS2017/2018		
Praktikum Technische Dynamik – Modellierung, Simulation und Experiment (MB, ME, WING, IP, BPT)		S. Leyendecker T. Bentaleb, D. Budday M. T. Duong, T. Gail T. Leitz, U. Phutane T. Schlögl, T. Wenger
Praktikum Matlab (MB)		M. Eisentraudt, T. Schlögl

Sommersemester 2017

Biomechanik (MT)		
Vorlesung + Übung		H. Lang
geprüft	34 + 6 (WS 2016/2017)	
Dynamik nichtlinearer Balken (MB, M, Ph, CE, ME, WING, IP, BPT)		
Vorlesung + Übung		H. Lang, T. Leitz
geprüft	19 + 1 (WS 2016/2017)	
Geometrische numerische Integration (MB, ME, WING, BPT)		
Vorlesung		S. Leyendecker
Übung		T. Wenger
geprüft	4 + 2 (WS 2016/2017)	
Statik und Festigkeitslehre (BPT, CE, ME, MWT, MT)		
Vorlesung		S. Leyendecker
Übung + Tutorium		D. Budday, M. Eisentraudt
geprüft	361 + 433 (WS 2016/2017)	T. Gail, T. Leitz J. Penner, U. Phutane T. Wenger
Theoretische Dynamik (TM, MB, ME, BPT, WING)		
Vorlesung + Übung		H. Lang, J. Penner
geprüft	34 + 5 (WS 2016/2017)	

Praktikum Rechnerunterstützte Produktentwicklung (RPE)
Versuch 6: Mehrkörpersimulation in Simulink (MB, ME, WING)
Teilnehmer 60 — D. Budday, T. Gail, M. T. Duong, T. Leitz, U. Phutane, T. Schlögl, T. Wenger

Additional exams

Numerische Methoden in der Mechanik
geprüft 6

Wintersemester 2016/2017

Biomechanik der Bewegung (MT)
Vorlesung + Übung — H. Lang
geprüft 24 + 5 (SS 2017)

Dynamik starrer Körper (MB, ME, WING, IP, BPT, CE)
Vorlesung — S. Leyendecker
Übung + Tutorium — D. Budday, D. Glaas
geprüft 407 + 126 (SS 2017) — T. Leitz, M. Ringkamp, U. Phutane, T. Schlögl

Mehrkörperdynamik (MB, ME, WING, TM, BPT, MT)
Vorlesung — S. Leyendecker
Übung — T. Wenger
geprüft 73 + 14 (SS 2017)

Numerische Methoden in der Mechanik (MB, ME, WING, TM, BPT, MT)
Vorlesung + Übung — H. Lang, J. Penner
geprüft 27 + 6 (SS 2017)

Theoretische Dynamik II (MB, ME, WING, TM, BPT, CE, M, Ph, LaP)
Vorlesung + Übung — H. Lang
geprüft 6

Dynamisches Praktikum – Modellierung, Simulation und Experiment (MB, ME, WING, IP)
Teilnehmer 15 — S. Leyendecker, H. Lang, D. Budday, T. Gail, U. Phutane, T. Leitz, M. Ringkamp, T. Schlögl, T. Wenger

4.4 Theses

Master theses

- Anika Kreipp
  MRT-Daten basierte geometrische Modellierung eines Rattenherzes

- David Holz
  Computing fibre orientations for a finite element model of a rat heart

- Ludwig Herrnböck
  Computational modelling of the cardiac electrophysiology of a rat left ventricle using finite elements

Project theses

- Björn König
  Simulation of a dielectric elastomer actuated revolute joint

- Kevin Lösch
  Finite element modelling of passive mechanical properties of a rat left ventricle

- Wuyang Zhao
  Variationaler Integrator für geregelte mechanische Systeme mit Zwangsbedingungen und impulsartigen Störungen

4.5 Seminar for mechanics

together with the Chair of Applied Mechanics LTM

27.01.2017 Wuyang Zhao
Project thesis, Chair of Applied Dynamics, University of Erlangen-Nuremberg
Variationaler Integrator für geregelte mechanische Systeme mit Zwangsbedingungen und impulsartigen Störungen

10.02.2017 Mahmood Jabareen
Faculty of Civil and Environmental Engineering, Technion, Haifa, Israel
A new approach for finite elements formulation using the Cosserat point theory

05.04.2017 Alexander Werner
Institut für Robotik und Mechatronik, Deutsches Zentrum für Luft- und Raumfahrt
Roboter auf zwei Beinen

04.05.2017 Miles B. Rubin
Faculty of Mechanical Engineering, Technion, Haifa, Israel
A new analysis of stresses in arteries based on a Eulerian formulation of growth in tissues

22.05.2017 Martin Grepl
Institut für Geometrie und Praktische Mathematik, RWTH Aachen
Reduced Basis Methods for Nonlinear Parametrized Partial Differential Equations

31.05.2017 Timo Heister
Mathematical Sciences, Clemson University, South Carolina
A parallel solution approach for crack propagation using adaptive mesh refinement

13.06.2017 Stephan E. Wolf
Junior Professor for Biomitic Materials and Processes, WW3, FAU
Bio-inspired functionally graded materials: process-structure-property relationships arising from nonclassical crystallization in vivo

12.07.2017 Claire Bruna-Rosso
Ph.D candidate, Politecnico di Milano
Finite Element Modeling of the Selective Laser Melting Additive Manufacturing Process

03.08.2017 Eleni Agiasofitou
Department of Physics, TU Darmstadt
Mathematical modelling of quasicrystals: generalized dynamics

16.08.2017 Anika Kreipp
Master thesis, Chair of Applied Dynamics, University of Erlangen-Nuremberg
MRT-Daten basierte geometrische Modellierung eines Rattenherzes

24.10.2017 Sonia Mogilevskaya
Department of Civil, Environmental, and Geo-Engineering, University of Minnesota
The Gurtin-Murdoch and Steigmann-Ogden models vis-á-vis the Benveniste-Miloh interface regimes

02.11.2017 David Holz
Master thesis, Chair of Applied Dynamics, University of Erlangen-Nuremberg
Computing fibre orientations for a finite element model of a rat heart

02.11.2017 Ludwig Herrnböck
Master thesis, Chair of Applied Dynamics, University of Erlangen-Nuremberg
Computational modelling of the cardiac electrophysiology of a rat left ventricle using finite elements

02.11.2017 Kevin Lösch
Project thesis, Chair of Applied Dynamics, University of Erlangen-Nuremberg
Finite element modelling of passive mechanical properties of a rat left ventricle

17.11.2017 Björn König
Project thesis, Chair of Applied Dynamics, University of Erlangen-Nuremberg
Simulation of a dielectric elastomer actuated revolute joint

08.12.2017 Wolgang Weber
Professur für Statik und Dynamik, Helmut-Schmidt-Universität/Universität der Bundeswehr Hamburg
Ein Ansatz zur Beschreibung des dynamischen Bewehrungsauszuges in Laminaten unter Verwendung einer Modellreduktion

4.6 Editorial activities

Advisory and editorial board memberships Since January 2014, Sigrid Leyendecker is a member of the advisory board of the scientific journal Multibody System Dynamics, Springer. She is a member of the Editorial Board of ZAMM – Journal of Applied Mathematics and Mechanics / Zeitschrift für Angewandte Mathematik und Mechanik since January 2016.

5 Publications

5.1 Reviewed journal publications

1. T. Schlögl, and S. Leyendecker. *A polarisation based approach to model the strain dependent permittivity of dielectric elastomers.* Sensors and Actuators, A: Physical, Vol. 267, pp. 156-163, 2017. DOI: 10.1016/j.sna.2017.09.048.

2. D. Budday, R. Fonseca, S. Leyendecker, and H. van den Bedem. *Frustration-guided motion planning reveals conformational transitions in proteins.* Proteins: Structure, Function, and Bioinformatics, Vol. 85, pp. 1795-1807, 2017. DOI: 10.1002/prot.25333.

3. A. Héliou, D. Budday, R. Fonseca, and H. van den Bedem. *Fast, clash-free RNA conformational morphing using molecular junctions* Bioinformatics, Vol. 33(14), pp. 2114-2122, 2017. DOI: 10.1093/bioinformatics/btx127.

4. T. Wenger, S. Ober-Blöbaum, and S. Leyendecker. *Construction and analysis of higher order variational integrators for dynamical systems with holonomic constraints.* Advances in Computational Mathematics, Vol. 43(5), pp. 1163-1195, 2017. DOI 10.1007/s10444-017-9520-5.

5. M. Ringkamp, S. Ober-Blöbaum, and S. Leyendecker. *On the time transformation of mixed integer optimal control problems using a consistent fixed integer control function.* Mathematical Programming, Vol. 161, pp. 1-31, 2017. DOI 10.1007/s10107-016-1023-5.

5.2 Invited lectures

1. D. Budday, R. Fonseca, A. Héliou, S. Leyendecker, and H. van den Bedem. *Revealing Molecular Mechanisms with Kino-Geometric Sampling (KGS).* Invited lecture, Kortemme Lab at UCSF, San Francisco, California, USA, 14 November 2017.

2. D. Budday, R. Fonseca, A. Héliou, S. Leyendecker, and H. van den Bedem. *Revealing molecular mechanisms through geometric rigidity analysis and motion planning.* Invited lecture, Gohlke group at Heinrich-Heine University, Düsseldorf, Germany, 31 July 2017.

3. S. Leyendecker. *Optimal control of human motion biological and artificial muscles* Workshop Computermodellierung von Wirbelsäule und Muskulatur, Koblenz, Germany, 28 March 2017.

5.3 Conferences and proceedings

1. D. Budday, R. Fonseca, S. Leyendecker, and H. van den Bedem. *Bridging protein rigidity theory and normal modes using kino-geometric analysis* Poster, BaMBA 11, UCSF, California, USA, 18 November 2017.

2. M.T. Duong, T. Wenger, L. Herrnböck, T. Ach, D. Holz, A. Kreipp, S.V. Binnewitt, H. Stegmann, S. Dittrich, M. Alkassar, and S. Leyendecker. *Modelling cardiac mechanics and electrophysiology of a rat left ventricle: A case study.* International Conference on Biomedical Technology, Hannover, Germany, 06-08 November, 2017.

3. J. Penner, T. Schlögl, and S. Leyendecker. *Optimal control of a slot car racer* Proceedings of the 7th GACM Colloquium on Computational Mechanics, Stuttgart, Germany, 11-13 October 2017.

4. T. Wenger, S. Ober-Blöbaum, and S. Leyendecker. *Higher order variational integrators for multirate and holonomically constrained systems.* International Conference on Scientific Computation and Differential Equations (SciCADE), Bath, UK, 11-15 September 2017.

5. D. Budday, R. Fonseca, S. Leyendecker, and H. van den Bedem. *Hierarchical, Structural Basis for Motions Encoding HDXMS Data* Poster, Conformational Ensembles from Experimental Data and Computer Simulations, Berlin, Germany, 25-29 August 2017.

6. T. Wenger, S. Ober-Blöbaum, and S. Leyendecker. *Mixed order variational integrators for multiscale problems.* Foundations of Computational Mathematics (FoCM), Barcelona, Spain, 10-12 July 2017.

7. T. Leitz, and S. Leyendecker. *On unit-quaternion based Galerkin Lie group variational integrators.* Foundations of Computational Mathematics (FoCM), Barcelona, Spain, 10-12 July 2017.

8. S. Björkenstam, J. Nyström, S.J. Carlson, M. Roller, J. Linn, L. Hanson, D. Högberg, and S. Leyendecker. *A framework for motion planning of digital humans using discrete mechanics and optimal control.* 5th International Digital Human Modeling Symposium/(eds.) Sascha Wischniewski & Thomas Alexander, Bonn, Germany, 26-28 June, 2017.

9. U. Phutane, M. Roller, S. Björkenstam, J. Linn, and S. Leyendecker. *Kinematic validation of a human thumb model.* ECCOMAS Thematic Conference on Multibody Dynamics, 10 Pages, Prague, Czech Republic, 19-22 June 2017.

10. M. Roller, S. Björkenstam, J. Linn, and S. Leyendecker. *Optimal control of a biomechanical multibody model for the dynamic simulation of working tasks.* ECCOMAS Thematic Conference on Multibody Dynamics, 10 Pages, Prague, Czech Republic, 19-22 June 2017.

11. T. Gail, S. Ober-Blöbaum, and S. Leyendecker. *Variational multirate integration in discrete mechanics and optimal control* ECCOMAS Thematic Conference on Multibody Dynamics, 10 Pages, Prague, Czech Republic, 19-22 June 2017.

12. H. Lang, and S. Leyendecker. *A generalised fourier method to solve the initial boundary value problem for free vibrating viscoelastic beam models.* ECCOMAS Thematic Conference on Multibody Dynamics, 10 Pages, Prague, Czech Republic, 19-22 June 2017.

13. T. Leitz, and S. Leyendecker. *Towards Higher Order Multi-Symplectic Lie-Group Variational Integrators for Geometrically Exact Beam Dynamics - Avoidance of Shear Locking.* ECCOMAS Thematic Conference on Multibody Dynamics, Prague, Czech Republic, 19-22 June 2017.

14. D. Glaas, and S. Leyendecker. *Variational integrator for constrained mechanical systems with pulsed disturbances and optimal feedback control.* GAMM Annual Meeting, Weimar, Germany, 6-10 March 2017.

15. U. Phutane, M. Roller, S. Björkenstam, and S. Leyendecker. *Investigating human thumb models via their range of motion volumes.* GAMM Annual Meeting, Weimar, Germany, 6-10 March 2017.

16. T. Wenger, S. Ober-Blöbaum, and S. Leyendecker. *Variational integrators of mixed order for constrained and unconstrained systems acting on multiple time scales.* GAMM Annual Meeting, Weimar, Germany, 6-10 March 2017.

17. T. Schlögl, and S. Leyendecker. *A polarisation based approach to model strain dependent electrostatic pressure of dielectric elastomer actuators.* GAMM Annual Meeting, Weimar, Germany, 6-10 March 2017.

18. J. Penner, T. Schlögl, and S. Leyendecker. *Optimal control of a slot car racer.* GAMM Annual Meeting, Weimar, Germany, 6-10 March 2017.

6 Social events

Visit of the Bergkirchweih 06.06.2017

Student summer party 27.07.2017

Visit of Felsengänge and Bowling Nuremberg 01.09.2017

Christmas party together with LTM 19.12.2016

Nikolaus hike 08.12.2016